CLASSIFICATION OF WIRELESS DEVICE LOCATION BASED ON Wi-Fi METADATA

A Thesis

by

PRANAY KUMAR EEDARA

Submitted to the Office of Graduate and Professional Studies of
Texas A&M University
in partial fulfillment of the requirement for the degree of

MASTER OF SCIENCE

Chair of Committee,	Jean-Francois Chamberland
Committee Members,	Gregory Huff
	Jiang Hu
	Rabi N. Mahapatra
Head of Department,	Miroslav M. Begovic

December 2016

Major Subject: Electrical Engineering

ABSTRACT

The advent of Wi-Fi infrastructures and wireless devices has changed the wireless landscape considerably. Of particular interest is Wi-Fi metadata, which provides information about the devices present in a wireless network and offers unintrusive ways in the inference of wireless device location and behavior. The Wi-Fi metadata of mobile devices can be obtained by deploying a network of monitoring devices over Wi-Fi. Monitoring devices consist of network interface cards in monitoring mode and are capable of listening to all Wi-Fi packets in the network traffic. This thesis examines the problem of estimating the occupancy of a region based on Wi-Fi metadata and compares the performance obtained with the data gathered by monitoring system with directional antennas to that of the same system with isotropic antennas. The monitoring antenna design is important because certain antenna radiation patterns can yield more discriminating information about current conditions.

In this work, occupancy estimation is formulated as a classification problem, and logistic regression and radial basis function networks are employed as the classification schemes. The metadata from Wi-Fi packets combined with received signal strengths from the monitoring antennas act as input to the classifiers. This work considers a specific scenario of occupancy estimation. The classification performance of the system is assessed with the synthetic data at different noise levels in the RSSI values, and with the experimental data obtained from a testbed implementation. The field data are acquired in a line-of-sight environment. The findings indicate that the judiciously selected directional

monitoring antennas work appropriately and significantly outperform the isotropic antennas in the scenario considered. This work introduces machine learning approaches for occupancy estimation based on Wi-Fi metadata and provides insight into the efficiency of directional antennas over isotropic antennas in the context of occupancy estimation. It also suggests that utilizing custom antenna designs based on the inference, shape and size of the target region can significantly improve the performance of a Wi-Fi monitoring system.

This dissertation work is dedicated to my family, my lab mates and friends for their guidance and support throughout the process.

ACKNOWLEDGMENTS

The work presented in this thesis was conducted in conjunction with Dr. Jean-Francois Chamberland, and it is intrinsically collaborative in nature. It benefited from an academic culture that promotes exchanges with other researchers at Texas A&M University.

I would like to thank my advisor Dr. Jean-François Chamberland for his continuous guidance, supervision and patience. His support throughout was invaluable. My sincere thanks to Dr. Gregory Huff, for his valuable advise and contribution in the design of antennas and practical implementations. I am grateful to his team at the Wireless Communications Laboratory, particularly to Hong Pan, David T. Grayson, and Danny Carey for their help and knowledge sharing in all phases of the work. I would like to thank my committee members - Dr. Jiang Hu and Dr. Rabi Mahapatra for their time, suggestions and interest in my thesis.

I thank the Texas A&M Transportation Services for allowing the field tests to take place in parking lot 100j. Special thanks to Hai Li, Mandel Oats, Austin Taghavi, Travis Taghavi, Nagaraj, Udaya Bhaskar, Keaton Brown and Thomas Branyon for their valuable support and participation in the field experiments.

NOMENCLATURE

MAC	Media Access Control
NUC	Intel's Next Unit of Computing device
RBF	Radial Basis Function
RF	Radio Frequency Signals
RSSI	Received Signal Strength Indicators

TABLE OF CONTENTS

LIST OF FIGURES

LIST OF TABLES

1 INTRODUCTION

The significant growth of mobile devices and the number of available Wi-Fi infrastructures have led to large amounts of data being transferred over wireless local area networks (WLANs). According to Cisco's Visual Networking Index [1], 41 percent of total internet traffic was transferred over Wi-Fi in 2014 and this figure is predicted to reach 53 percent by 2019. Cisco's forecast of the growth in Wi-Fi traffic is depicted in Fig. 1.1 [1]. It also indicates that, in mobile devices with both cellular and Wi-Fi connectivity, a major proportion of the mobile data is being offloaded from expensive cellular networks onto lower cost Wi-Fi networks. The traffic in a Wi-Fi network can be passively monitored by deploying a set of low cost Wi-Fi monitoring units. Wi-Fi packets contain information about the media access control (MAC) address of the transmitter, and this information can be augmented by the signal strength measured at the monitoring device. As such, received signal strengths can act as an indication of signal propagation distance and they, thereby, provide partial information about the physical location of the transmitter.

In addition, active wireless devices periodically transmit certain packets, like probe requests or response frames, to obtain information about nearby access points or to check the quality of their connections. This implicitly makes Wi-Fi enabled devices reveal their presence through radio frequency (RF) signals. These properties of Wi-Fi traffic and radio frequency signals offer unintrusive ways to perform several inference tasks on the physical world. In this work, we are interested in the inference task of estimating a wireless device's

physical confinement relative to an enclosed area based on received signal strengths.

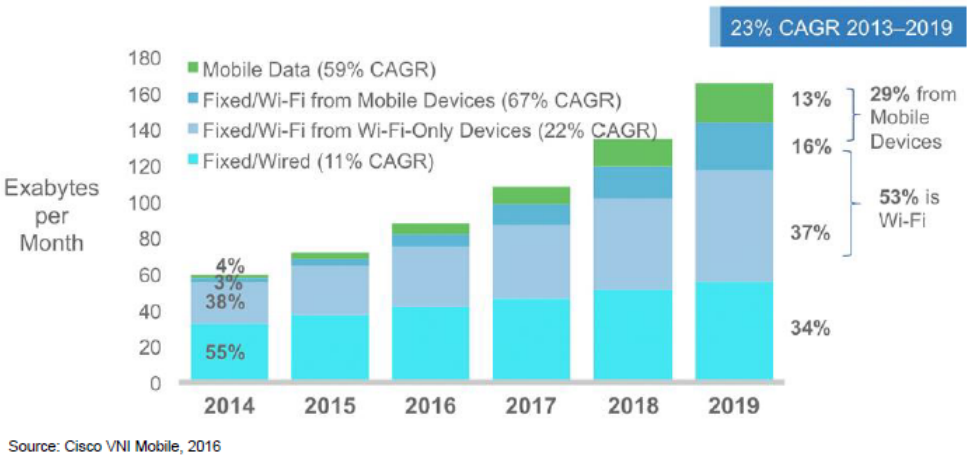

Figure 1.1: Cisco's forecast of Wi-Fi traffic growth

1.1 Literature Review

RF signal based inference tasks have gained the interest of researchers over the past decades due to their unique characteristics and wide range of applications. Currently, there exists a vast amount of literature on these tasks, e.g., [2, 3, 4, 5, 6]. These research contributions illustrate the ability to infer a physical location based on Wi-Fi signals. Radio frequency signals are used in inference tasks like self-localization, source localization and network structure inference [7, 8, 9, 10, 11, 12, 13]. The information afforded by these inference tasks has been used in applications ranging from targeted advertising in marketing campaigns to robotic systems.

In this thesis, we examine the related problem of occupancy estimation based on Wi-Fi activity. Occupancy estimation refers to the problem of estimating the number of

active devices inside a room or a building. This is intrinsically connected to the problem of finding the physical confinement of a mobile device relative to a prescribed area based on received signal strengths. The estimates of room occupancy offer a lot of benefits in various applications ranging from smart home management, emergency response operations to marketing research and analysis [14, 15]. For instance, it can save considerable energy by automatic optimization of heating and cooling systems. It provides cost effective ways to estimate the size of audiences at conferences and symposia. Readings from monitoring sensors can be used to control wireless infrastructures by making decisions on activating or de-activating access points.

Current work on estimating room occupancy is either based on cameras [16, 17] or RF signals. The use of camera based approaches result in high installation costs and are limited by practical aspects such as occlusion, lighting, camera height and angles. On the other hand, occupancy estimation based on RF signals leverages existing infrastructures, and it is the focus of recent work [18, 19]. Some RF-signal-based approaches rely on wireless devices carried by the users while others are device free. Device based approaches assume that every person carries a Wi-Fi enabled device and they are prone to errors. These approaches are nevertheless applicable to most scenarios as estimates of room occupancy need not be exact, only their error should be in a tolerable range. In this work, occupancy estimation based on RF devices carried by the users is the prime consideration. The focus is on evaluating the performance of this monitoring task under different sensing antenna designs.

The inference in a wireless monitoring system is based upon the information gathered by its sensing devices. In these systems, the ability to conduct an inference task is closely linked to the design of its sensing devices. The research work in the field of metrology illustrates how important it is to design sensing devices specific to an application scenario [20, 21]. Similarly, the design of sensing antennas used for RF monitoring can play a determinant role in the performance of an overall system. In the antennas and propagation community, the effect of antenna radiation patterns is well understood as it fuels a large part of their research in radar, communication and other applications. However, the impact of their operating characteristics is not yet fully studied in the design and analysis of RF monitoring based inference systems. In the communications and signal processing literature, RF antennas are primarily viewed as a commodity and their potential for increased performance is often overlooked. Although commercial RF antennas are designed for wireless communication, custom antennas can be tailored to a monitoring task for improving its performance. Furthermore, as reconfigurable antenna technology evolves and proliferates, a wireless inference system can adapt to dynamic environments or objectives. This thesis addresses this knowledge gap by examining potential antenna designs and characterizing their impact on the particular monitoring task of occupancy estimation.

1.2 Wi-Fi Monitoring

The mobile devices present in a region of interest can be detected by monitoring the traffic in the wireless local area networks. The packets transmitted in these networks

follow a protocol defined in the IEEE 802.11 standard. According to this standard, every frame in the network includes of an individual MAC address of the immediate transmitter. Individual MAC addresses serve as the unique identifier for a device. Wireless devices with enabled Wi-Fi network cards periodically send/receive certain management frames like probe request or response frame to get information about active APs. Consequently, all active devices can be identified by counting the total number of distinct MAC addresses present in the network traffic.

The transmitted data packets in a Wi-Fi network are monitored using certain wireless network cards like Alfa™ `AWUS036NHA`. These network cards are composed of a detachable antenna and a chipset. The chipset provides two modes of operation: Managed and Monitor. The Managed mode is the default mode of any network card while connected to a network for data transfer. In this mode, the network card only listens to the packets that are aimed at this device. The Monitor mode, also known as Promiscuous mode, allows capturing of all packets present on a particular channel in the network. The network card augments the captured frames with additional information like received signal strengths for subsequent analysis. The MAC address of the transmitter and the corresponding RSSI values can be deciphered using application programming interfaces like `pcap` and `WinPcap` or fully-featured programs such as Wireshark and Kismet. This is depicted in Fig. 1.2. The detachable antenna in the network card can be replaced with custom designed antennas by utilizing a reverse polarity subminiature version A (RP-SMA) antenna connector. This allows monitoring with a custom designed antenna.

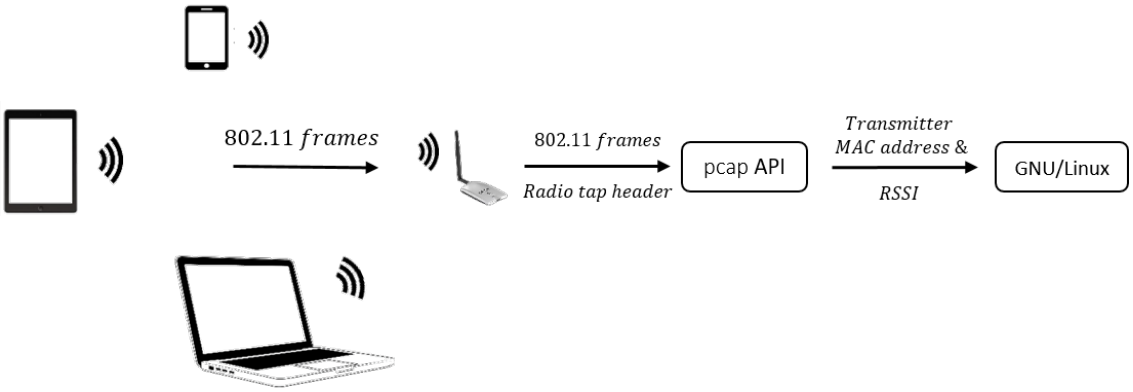

Figure 1.2: This diagram illustrate a monitoring system based on Wi-Fi packets.

In practice, the inference task is performed over a single monitoring period and the captured packets may also contain large portion of irrelevant devices like static devices and access points. Static devices with Wi-Fi interfaces are easy to identify from historical data because they are essentially immobile for large periods of time and they tend to be active throughout the day. The corresponding addresses and strength readings can be eliminated from the gathered data with very high confidence through blacklisting. Access Points can also be blacklisted using the beacon frames transmitted by them. It is therefore possible to obtain the total number of active mobile devices present about the region of interest by deploying sensing devices around it.

The Wi-Fi packets acquired by the monitoring antennas are not confined to the devices within the target area; they may be coming from transmitters that are located outside the region of interest. This is due to the propagation characteristics of electromagnetic waves. Thus, the classification of the observed device locations is required. In the envisioned setting, multiple distributed agents are used over the prescribed area of interest

for RF monitoring. The data acquired by these monitoring units is aggregated over the Internet, and the classification of observed devices is performed at the central location.

1.3 Received Signal Strengths

The wireless devices observed by a distributed monitoring system are classified based on their signal strengths received at multiple sensing units. The power of a RF signal decays with the distance from the transmitting agent. This characteristic of RF signal provides partial information about the whereabouts of the transmitting agent. In a wireless environment, the signal strength received at a monitoring device depends on multitude of factors. The RF signal power is effected by noise, interference, antenna orientation and other channel obstacles such as shadow fading. In this work, we assume that the energy captured by a monitoring device comes primarily from a line-of-sight path. Over short distances, the signal strength of the electromagnetic wave coming from this agent is governed by the free-space path loss. In this thesis, received signal strength is modeled using the free-space path loss equation.

1.4 Thesis Contribution

This thesis revisits occupancy estimation, while giving due consideration to the radiation characteristics of the sensing antennas. The objective is to evaluate the classification of observed wireless devices with the data obtained from directional and omni-directional antennas. This work formulates the occupancy estimation as a classification task. Wireless devices observed by a Wi-Fi monitoring system are classified relative to an enclosed

area of interest, i.e., inside or outside, to obtain occupancy estimates. The classification is based on the signal strengths received at multiple monitoring units. For classification, several competing statistical and machine learning methods are considered. This framework allows for the study of the correlation between performance and RF signal analysis. This thesis also provides an opportunity to better understand the potential advantages of using reconfigurable antennas in monitoring systems.

1.5 Thesis Organisation

The remainder of the thesis is organized as follows. In Chapter II, we illustrate the envisioned framework of the inference task through a notional diagram and formulate the occupancy estimation as a binary classification problem. The two classification schemes, namely logistic regression and radial basis function networks, employed in this work are discussed in Chapter III. In Chapter IV, we describe the simulation setup and survey the potential antenna designs employed in this work. We also describe the procedure employed for generating synthetic data sets for monitoring systems with directional and isotropic antennas. Simulation results are presented in this chapter for comparing the performance of classifiers with different sensing systems. To complement the findings from numerical simulations, an experimental campaign is conducted in a line-of-sight environment to acquire field data. Chapter V provides a brief description of this experimental setup and discusses our experimental findings. Finally, we provide insights, conclusions and possible extensions in Chapter VI.

2 PROBLEM FORMULATION

The occupancy estimation based on Wi-Fi activity of the users can be formulated as estimating the total number of active wireless agents in the prescribed area of interest. In the proposed framework, we consider the area of interest to be a region inscribed in a larger region and for simplicity, we consider the inscribed region and outer region to be rectangular areas. Let area of the target region and outer region be denoted by $\mathscr{A}_{\mathrm{t}}$ and $\mathscr{A}_{\mathrm{o}}$, respectively. In general, wireless devices carried by the users are randomly located within the overall area. This implies the presence of devices in the target region and in the outer region. Sensing devices deployed around the area of interest capture transmitted packets from all these devices. In practice, the monitoring range of the sensing devices determines the area of the outer region. Figure 2.1 shows a notional diagram for this framework.

The objective is to identify the devices belonging to the region of interest from the vector of observed devices. This can be achieved by classifying the observed wireless devices into one of the two regions. In the envisioned setting, the Wi-Fi monitoring units are placed in an arbitrary fashion around the target region, and they are aware of their location and radiation characteristics of the sensing antenna. Each sensing device extracts the MAC address and an RSSI measurement for every monitored packets. It subsequently relays this information to the central server over the Internet. At the central server, each wireless device is identified by its unique MAC address; RSSI values belonging to a particular device are grouped together based on its MAC address. Each wireless device is then classified as

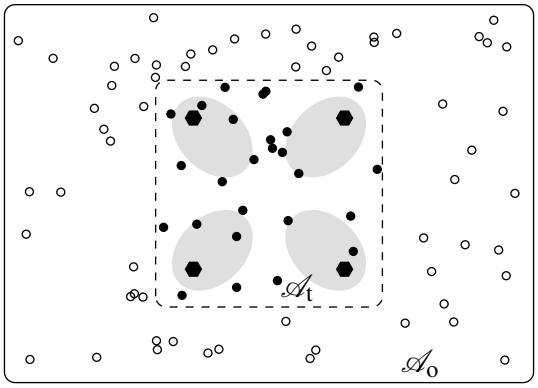

Figure 2.1: Notional diagram illustrating the inference task. The periphery of target area is delineated by dashed line. Hexagons denote the locations of monitoring devices, equipped with directional antennas. Agents within the zone of interest are in black, whereas outside agents appear as circles. The objective is to estimate occupancy within target area.

belonging to the target region or outer region based on the RSSI information fused from all the sensing devices. The total number of active wireless agents in the region of interest is estimated by counting all the wireless devices classified to be in the target region.

In this study, we assume that the wireless users are quasi-static and an inference task is performed over a single monitoring period. Although it is possible to incorporate moving agents and streaming observations into the problem formulation, these features render the analysis more challenging and they are not necessary to achieve our goal of better understanding the interplay between antenna profiles and RF monitoring. As such, advanced mobility models and their ramifications are relegated to future work in favor of a simpler, explicative model suited to our main purpose. For convenience, the random locations of the wireless devices are aggregated into a single vector, $\underline{\mathbf{U}} = (\mathbf{U}_1, \ldots, \mathbf{U}_{n_\mathrm{a}})$. Wireless agents are equipped with vertically polarized, isotropic antennas. The power radiated by one agent is therefore uniform in all directions on the plane. The transmit

power for every mobile agent is known and equal to the limit prescribed by the Federal Communications Commission (FCC) for the industrial, scientific and medical (ISM) radio bands.

For the purpose of analysis, we assume that the energy captured by a monitoring device comes primarily from a line-of-sight path. Over short distances, the signal strength of the electromagnetic wave coming from this agent is governed by the free-space path loss. The received signal strength from source j to sensing unit i can be expressed as

$$P_{ij}[\text{dBm}] = A + B\log_{10}(d_{ij}) + L_{ij} + G_i(\phi_{ij}) \tag{2.1}$$

where A and B are the mean decay parameters, d_{ij} represents the Euclidean distance between the source and the measurement device, L_{ij} denotes shadow fading, and $G_i(\cdot)$ is the antenna gain of the sensing unit. Explicitly, suppose that the sensing agent is located at point $\mathbf{s}_i = (s_{1i}, s_{2i})$ and the signal originates from $\mathbf{u}_j = (u_{1j}, u_{2j})$; then, the distance between the two points is equal to

$$d_{ij} = d(\mathbf{s}_i, \mathbf{u}_j) = \|\mathbf{u}_j - \mathbf{s}_i\|_2 = \sqrt{(u_{1j} - s_{1i})^2 + (u_{2j} - s_{2i})^2}.$$

Likewise, the angle of incidence of the electromagnetic wave onto the sensing unit is given by

$$\phi_{ij} = \angle(\mathbf{s}_i, \mathbf{u}_j) = \text{atan2}(u_{2j} - s_{2i}, u_{1j} - s_{1i}),$$

where $\text{atan2}(\cdot,\cdot)$ is the two-argument variant of the arctangent function. The antenna gain $G_i(\cdot)$[dB] may depend on the antenna characteristics of device i, its current orientation, the angle of incidence of the incoming signal, and its polarization.

The shadow fading components $\{L_{ij}\}$ are assumed to form a set of independent and identically distributed random variables, each with a log-normal distribution. In the logarithmic domain, the probability density function common to all fading components, $\{L_{ij}\}$, is

$$f_{L_{ij}}(\ell) = \frac{1}{\sqrt{2\pi}\sigma_{\mathrm{s}}} \exp\left(-\frac{\ell^2}{2\sigma_{\mathrm{s}}^2}\right) \tag{2.2}$$

where σ_{s} is the logarithmic standard deviation of the shadowing, expressed in natural units.

The observed information available at the fusion center for the purpose of inference takes the form of a sequence of vectors $\underline{\mathbf{P}} = (P^{(1)}, \ldots, P^{(n_{\mathrm{a}})})$, with each information vector corresponding to a particular mobile agent. The length of vector element $\mathbf{P}_j$ corresponds to the total number of sensing devices monitoring the field of interest. Its entries are the signal strengths captured by the sensors, $P^{(j)} = (P_1^{(j)}, \ldots, P_{n_{\mathrm{s}}}^{(j)})$, where n_{s} is the number of monitoring devices. The fusion center possesses side information in the form of the locations of sensing devices, their orientations and antenna properties.

The classification of wireless device locations based on received signal strengths is achieved by using supervised machine learning algorithms. The observed information available for the purpose of classification takes the form of $P = (P_1, \ldots, P_{n_{\mathrm{s}}})$ where n_{s} represents the number of sensing devices and its elements correspond to the signal strength received by the monitoring antennas. The classification problem can be stated as estimating the probability of a wireless agent belonging to one of the regions conditioned on the observed signal strengths P,

$$\Pr(Y|P)$$

where Y represents a binary variable that takes the value of 1 if it belongs to the region of interest and -1 if it belongs to the outer region.

3 CLASSIFICATION SCHEMES

This section gives an overview of the classification schemes employed in this work. Logistic regression and radial basis function networks are considered for classifying the region of a wireless device based on the set of received signal strengths. In these methods, the classification rule is learned by training the model with a set of examples. The input for the classifier is the power vector $P = (P_1, \ldots, P_{n_s})$ received from all the monitoring sensors and the classifier output Y represents a binary variable that takes the value of 1 if it belongs to the region of interest and -1 if it belongs to the outer region.

3.1 Logistic Regression

Logistic regression is a widely used learning algorithm for classification. In logistic regression, the hypothesis h used for classification is represented using a sigmoid function,

$$h_\theta(P) = g(\theta^T P) = \frac{1}{1 + e^{-\theta^T P}}.$$

The output of the hypothesis function is interpreted as the probability of a wireless device belonging to a region conditioned on the set of observed signal strengths and parameterized by θ,

$$h_\theta(P) = \Pr(Y = 1 | P; \theta).$$

Logistic regression predicts a wireless device to be in the target region whenever $h_\theta(P)$ is greater than 0.5 and this happens when $\theta^T P \geq 0$. The objective is to find a set of parameters, θ, such that the product $\theta^T P$ can be used to determine whether the features

P are the result of a positive or negative sample, i.e., $Y = 1$ or $Y = -1$. As a supervised learning algorithm, the parameter vector θ of the hypothesis function is learned by fitting a set of training data to the logistic function. The learning involves the minimization of the associated cost function $J(\theta)$ given by

$$J(\theta) = \frac{1}{M} \sum_{i=1}^{M} \text{Cost}(h_\theta(P^{(i)}), Y_i)$$

where

$$\text{Cost}(h_\theta(P^{(i)}), Y_i) = \begin{cases} -\ln(h_\theta(P^{(i)})) & \text{if } y = 1 \\ -\ln(1 - h_\theta(P^{(i)})) & \text{if } y = 0. \end{cases}$$

Variable M is the number of training samples and $P^{(i)}$ is the power vector received for the i^{th} sample. The cost function $J(\theta)$ is minimized using the gradient descent method.

Assume that we have the training set with features $\mathbf{P} = (P^{(1)}, P^{(2)}, \ldots, P^{(M)})$, with $P^{(i)} \in \mathbb{R}^{n_s}$; and the associated target results $\mathbf{Y} = (Y_1, Y_2, \ldots, Y_M)$, where $Y_i \in \{0, 1\}$. Given an initial guess of $\theta \in \mathbb{R}^n$,

$$\Pr(Y_i = 1 | P^{(i)}) = \text{logit}(\theta^T P^{(i)}) = \frac{1}{1 + e^{-\theta^T P^{(i)}}} = h_\theta(P^{(i)}).$$

This $h_\theta(P^{(i)})$ can then be thresholded at 0.5 to classify any set of features as inside or outside. To evaluate the effectiveness of this θ, we look at the cost function $J(\theta)$.

Overall, the θ that minimizes $J(\theta)$ for a given training set $\mathbf{P}$ and $\mathbf{Y}$ is called the learned set of parameters. This set of parameters can then be used along with the logistic function and a set of observed features to estimate the probability that the set was the result of a 1, which can then be used to classify the set as the result of a 0 or 1.

Importantly, the decision boundary learned by the logistic regression is linear in the

observed feature vector space. The regression does not need to rely on only observed features. Since the estimation is based on a function of a linear combination of the features, the non linear decision boundaries can be learned by creating synthetic features from one or more of the observed features using non-linear functions . For example, it may be useful to take powers or products of various observed features. Other common regression problems such as overfitting/underfitting are also potentially present with logistic regression.

3.2 Radial Basis Networks

The non-linear decision boundaries in the input vector space can also be learned by using radial-basis function networks. The key idea is that the decision boundaries are more likely to be linear in the high dimensional space than in the low-dimensional space. The low dimensional input vectors are mapped onto high dimensional feature vectors f using the kernel functions. A widely used kernel is the multivariate Gaussian distribution. Given an input vector P and a center t in the input vector space, the similarity function or Gaussian kernel is defined as

$$\text{similarity}(P,t) = K(P,t) = \exp\left(-\frac{\|P-t\|^2}{2\sigma^2}\right).$$

The high dimensional feature vector f is linearly combined with the parameter or weight vector θ to obtain the decision boundary. In this approach, the hypothesis function $h_\theta(f)$ does not output the probabilities, instead it outputs 1 when $\theta^T f \geq 0$ and -1 when $\theta^T f < 0$,

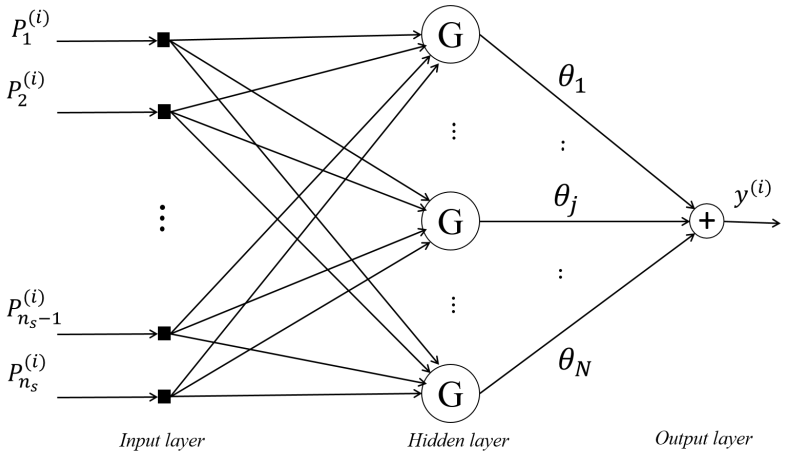

Figure 3.1: Radial basis function network.

i.e.,

$$h_\theta(f) = \begin{cases} 1 & \text{if } \theta^T f \geq 0 \\ -1 & \text{if } \theta^T f > 0 \end{cases}$$

This notion is presented using radial basis function networks. The network consists of three layers with entirely different roles. The input layer is made up of source nodes equal to the dimension of the input vector. The second layer in the network is known as the hidden layer. It is composed of nodes with radial basis functions and each hidden layer node is directly connected to all the input layer nodes. The number of hidden layer nodes is greater than the dimension of the input vector. The hidden layer maps the input vector to a high dimensional feature vector using radial basis functions. The output layer supplies the response by linearly combining the high dimensional feature vector. The RBF network structure is shown in Fig. 3.1

The input to the radial basis network is represented using a column vector $P^{(i)} =$

$[P_1,\ldots,P_{n_s}]^T$. The column vector $P^{(i)}$ corresponds to the power vector of the i^{th} observed device. The total number of monitoring devices n_s determines the number of nodes in the input layer. In the hidden layer, the output of the j^{th} node is given by $G(P^{(i)},t_j)$ where t_j is the center vector of the j^{th} unit,

$$\begin{aligned} G\left(P^{(i)},t_j\right) &= G\left(\|P^{(i)}-t_j\|_{C_j}\right) \\ &= \exp\left(-(P^{(i)}-t_j)^T {C_j}^T C_j (P^{(i)}-t_j)\right) \\ &= \exp\left(-\frac{1}{2}(P^{(i)}-t_j)^T {\Sigma_j}^{-1}(P^{(i)}-t_j)\right). \end{aligned}$$

where the norm weighing matrix C_j and inverse matrix ${\Sigma_j}^{-1}$ are defined by

$$C_j = \begin{bmatrix} \frac{1}{\sqrt{2}\sigma_{j1}} & 0 & 0 & \cdots & 0 \\ 0 & \frac{1}{\sqrt{2}\sigma_{j2}} & 0 & \cdots & 0 \\ \vdots & \vdots & \vdots & \ddots & \vdots \\ 0 & 0 & 0 & \cdots & \frac{1}{\sqrt{2}\sigma_{jn_s}} \end{bmatrix},$$

$${\Sigma_j}^{-1} = 2 * {C_j}^T C_j = \begin{bmatrix} \frac{1}{{\sigma_{j1}}^2} & 0 & 0 & \cdots & 0 \\ 0 & \frac{1}{{\sigma_{j2}}^2} & 0 & \cdots & 0 \\ \vdots & \vdots & \vdots & \ddots & \vdots \\ 0 & 0 & 0 & \cdots & \frac{1}{{\sigma_{jn_s}}^2} \end{bmatrix},$$

where σ_j is the spreads associated with the center vector t_j. The dimension of the center vector t_j is equal to the dimension of the input vector as the center vector lies in the input vector space.

The output layer consists of only one node and its response for the i^{th} sample is given

by $y^{(i)}$,

$$y^{(i)} = \sum_{j=1}^{N} \theta_j G\left(\|P^{(i)} - t_j\|_{C_j}\right)$$

where N represents the number of basis functions in the hidden layer, the parameter vector $\theta = [\theta_1, \theta_2, \ldots, \theta_j, \ldots, \theta_N]$ is a column vector of dimension $N \times 1$, and it consists of the weights associated with the output layer of the network. Typically, in the generalized radial basis networks, the number of nodes or basis functions in the hidden layer (N) is less than the number of samples in the training set (M), i.e., $N < M$.

In the RBF network, the error associated with the i^{th} training sample is represented as er_i and is defined by

$$er_i = d_i - y^{(i)} = d_i - \sum_{j=1}^{N} \theta_j G(\|P^{(i)} - t_j(n)\|_{C_j})$$

where d_i is the desired output of the i^{th} training sample.

In the generalized RBF network of Fig. 3.1, the weight vector θ associated with the output layer, the positions of the center vector t of the radial-basis functions, and the inverse matrix Σ^{-1} related to the norm weighing matrix C_j are all unknown parameters that must be learned. There are different learning strategies that can be followed in the design of an RBF network, depending on how the centers of the radial-basis functions of the network are specified. In this work, the centers of the radial-basis functions and all other free parameters of the network undergo a supervised learning process, i.e., the RBF network takes on its most generalized form. The error-correction learning is based on the gradient descent procedure.

In the gradient decent method, the cost function J of the RBF network is defined to

Procedure 1: Gradient Descent Procedure for the RBF Network

1 Update of linear weights in output layer

$$\frac{\partial J(n)}{\partial \theta_j(n)} = \sum_{i=1}^{M} er_i(n) G\left(\|P^{(i)} - t_j(n)\|_{C_j}\right)$$

$$\theta_j(n+1) = \theta_j(n) - \eta_1 \frac{\partial J(n)}{\partial \theta_j(n)} \quad j = 1, 2, \ldots, \mathbf{N}.$$

2 Update of centers in hidden layer

$$\frac{\partial J(n)}{\partial t_j(n)} = 2\theta_j(n) \sum_{i=1}^{M} er_i(n) G'\left(\|P^{(i)} - t_j(n)\|_{C_j}\right) {\Sigma_j}^{-1} \left[P^{(i)} - t_j(n)\right]$$

$$t_j(n+1) = t_j(n) - \eta_2 \frac{\partial J(n)}{\partial t_j(n)} \quad j = 1, 2, \ldots, \mathbf{N}.$$

3 Update of spreads of centers in hidden layer

$$\frac{\partial J(n)}{\partial {\Sigma_j}^{-1}(n)} = -\theta_j(n) \sum_{i=1}^{M} er_i(n) G'\left(\|P^{(i)} - t_j(n)\|_{C_j}\right) Q_{ji}(n)$$

$$Q_{ji}(n) = \left[P^{(i)} - t_j(n)\right] \left[P^{(i)} - t_j(n)\right]^T$$

$${\Sigma_j}^{-1}(n+1) = {\Sigma_j}^{-1}(n) - \eta_3 \frac{\partial J(n)}{\partial {\Sigma_j}^{-1}(n)} \quad j = 1, 2, \ldots, \mathbf{N}.$$

Above:
M - Total number of training samples.
N - Total number of basis functions present in the hidden layer
η - Learning rate of the update equation
$\theta(n)$ - Weight vector θ during the n^{th} training iteration
$G'(\cdot)$ - First derivative of the function $G(\cdot)$ with respect to its argument.

minimize the mean squared error for a given set of training data and is given by

$$J = \frac{1}{2}\sum_{i=1}^{M} er_i^2$$

where M is the total number of training samples and er_i represents the error associated with the i^{th} training sample.

The gradient descent is an iterative method. It learns the optimal parameters by iteratively updating them. The update equations involved in the gradient decent procedure are shown in Procedure 1. The update equations for θ, t , and Σ^{-1} are assigned different learning-rate parameters η_1, η_2 and η_3 respectively. The linear weights associated with the output layer of the network tend to evolve on a different time scale compared to the nonlinear activation functions of the hidden units. In general, the learning-rate of the weight vector is chosen to be greater than the learning-rates of the hidden layer parameters. Thus, as the hidden layer's activation functions evolve slowly in accordance with some optimization strategy, the output layer's weights adjust themselves rapidly through a linear optimization strategy. The gradient descent method terminates the update of the parameters when the curve of mean squared error converges.

The cost function of the RBF network is convex with respect to the weight parameter θ, but nonconvex with respect to the centers t and matrix Σ^{-1}; in the latter case, the search for the optimum values of t and Σ^{-1} may get stuck at a local minimum in parameter space. For the initialization of the gradient-descent procedure, it is often desirable to begin the search in parameter space from a structured initial condition that limits the region of parameter space to be searched to an already known useful area. In doing so, the likelihood

of converging to an undesirable local minimum in weight space is reduced.

4 NUMERICAL SIMULATIONS

The objective of numerical simulations is to evaluate the classification performance of the logistic regression and RBF networks discussed in the previous chapter with the data obtained from monitoring systems with different antenna designs. Simulations are performed for a particular configuration of the framework considered in the problem formulation, i.e., for a particular number, position and orientation of the monitoring devices. This chapter discusses the framework employed in the simulations, the data sets used for performance evaluation, and the numerical findings.

4.1 Simulation Framework

In the simulation framework, the target area $\mathscr{A}_\mathrm{t}$ is considered to be a square of dimension 20 m $\times$ 20 m inscribed in a larger square of dimension 50 m $\times$ 50 m. The monitoring system consists of four monitoring devices placed at the corners of the region of interest. The sensing antennas of the monitoring units point towards the center of the target region. This configuration of pointing directions creates discriminating patterns for the directional antennas. For every wireless device present within the overall monitoring region, a vector of four RSSI values is acquired, one per monitoring unit. This power vector is supplied as input to the classifiers to obtain the region associated with the wireless device, i.e., inside or outside.

4.1.1 Antenna Designs

To analyze the effect of radiation characteristics of the sensing antennas on the classification, isotropic antennas and directional antennas with 3 dB beamwidth $\theta_{3\text{dB}} = 90^\circ$ are considered. General trends extend to other directional antennas. The radiation characteristics of these antennas are depicted in Fig. 4.1. The gain $G_i(\cdot)$ of a directional antenna is established using the 3GPP antenna model [22]. Each radiation pattern is characterized by a pointing direction of maximum gain and a beamwidth. Mathematically, we have

$$G_i(\phi_{ij}) = -\min\left\{12\left(\frac{\phi_{ij}-\theta_i}{\theta_{3\text{dB}}}\right)^2, G_{\text{floor}}\right\} - G_{\text{avg}}$$

where $\theta_i \in (-180^\circ, 180^\circ]$ is the pointing direction (boresight) of the antenna attached to unit i; $\theta_{3\text{dB}}$ is the 3 dB beamwidth of this radiation pattern in degrees; and G_{floor} is a nominal attenuation floor. The last variable G_{avg} is a normalization factor that enables a fair comparison between distinct antennas. Normalization constant G_{avg} ensures that all antennas radiate the same amount of power; its value is proportional to the average antenna gain

$$10\log_{10}\left(\int_{-180}^{180}\frac{10^{-\frac{1}{10}\min\left\{12\left(\frac{\phi_{ij}-\theta_i}{\theta_{3\text{dB}}}\right)^2, G_{\text{floor}}\right\}}}{360}d\phi_{ij}\right).$$

The gain associated with isotropic antennas is uniform and zero.

4.1.2 Synthetic Data

To generate the synthetic data for performance evaluation, the overall area is divided into a grid of 0.5 m $\times$ 0.5 m and the power vector received from the four monitoring units is generated at all the points in the grid using the free space path loss equation. According

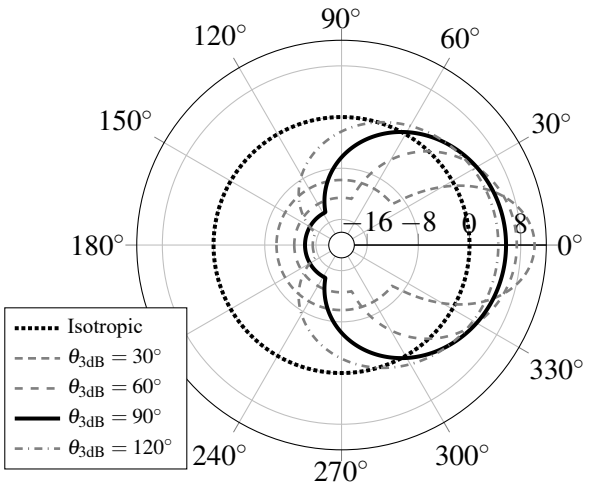

Figure 4.1: This graph depicts normalized antenna radiation patterns for various 3 dB beamwidths.

to it, the received signal strength from source j to sensing unit i can be expressed as

$$P_{ij}[\text{dBm}] = A + B\log_{10}(d_{ij}) + L_{ij} + G_i(\phi_{ij}) \tag{4.1}$$

where A and B are the mean decay parameters, d_{ij} represents the Euclidean distance between the source and the measurement device, L_{ij} denotes shadow fading, $G_i(\cdot)$ is the antenna gain of the sensing unit and ϕ_{ij} is the angle of incidence.

In (4.1), the values of the physical parameters A and B are chosen to be 19.73 and -20, respectively. These values are based on the regulation by Federal Communications Commission (FCC) and the profile of typical wireless environments. Using these parameter values, three data sets with 10,000 points each are generated for directional antennas and isotropic antennas by varying noise levels in the shadow fading component. The noise is generated using the normal distribution with different standard deviations. Each data set contains the power vectors from all the points in the grid and the corresponding region of

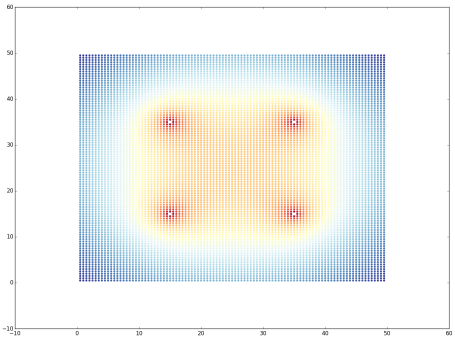

(a) Directional with 0 db noise.

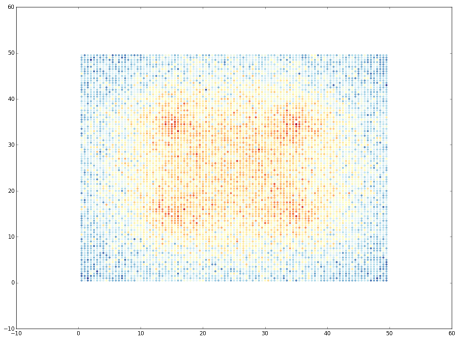

(b) Directional with 4 db noise.

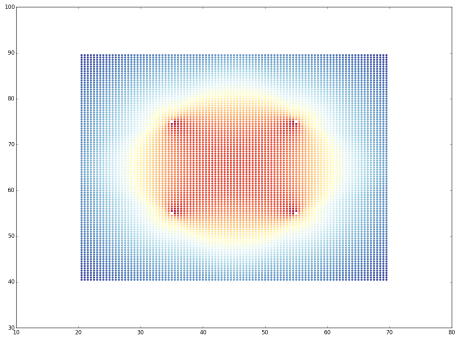

(c) Omnidirectional with 0 db noise.

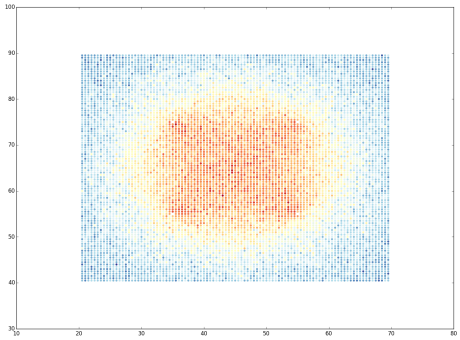

(d) Omnidirectional with 4 db noise.

Figure 4.2: Heatmaps of the data sets used for training the classifiers. The value at each location is the sum of the powers received at the four monitoring devices from that location.

the points. The data sets are stored in the form of an SQLite database. The heat maps of the data sets generated are shown in Fig. 4.2.

4.2 Simulation Results

The data sets are normalized before training the classifiers. After normalization, 80 percent of the data is randomly chosen for training and validation of the classifier, and 20 percent of the data is used for testing.

The design choices or hyper parameters involved in the RBF network are the number of radial basis functions in the hidden layer N and the learning rates η_1, η_2 and η_3 of the weight vector θ, the center vectors t and the inverse matrix Σ^{-1} ,respectively. The gradient descent method starts with an initialization of θ, t and Σ^{-1}, and iteratively updates them until the optimal parameters are reached in the search space. In practice, the termination of the parameter updates is determined using the learning curve, which is a plot of the mean-square value of the error versus the number of iterations n. The learning curve starts from a large value determined by the initial conditions for θ, t & Σ^{-1}, and then decreases at some rate depending on the update equations and the values of the learning rates. It eventually converges to a steady state value. The optimal parameters obtained with the training are used for testing.

The hyper parameters chosen for the RBF network for different data sets are shown in Table 4.1. The noise levels 0db, 2db and 4db represent the standard deviations of the normal distribution in the logarithmic domain. The hyper parameters are chosen based on

Table 4.1: Hyper parameters of the RBF network.

Antenna	**Noise Level**	N	η_1	η_2	η_3
directional	0db	10	0.05	0.02	0.02
directional	2db	10	0.05	0.02	0.02
directional	4db	10	0.05	0.02	0.02
isotropic	0db	15	0.06	0.03	0.03
isotropic	2db	15	0.06	0.03	0.03
isotropic	4db	15	0.06	0.03	0.03

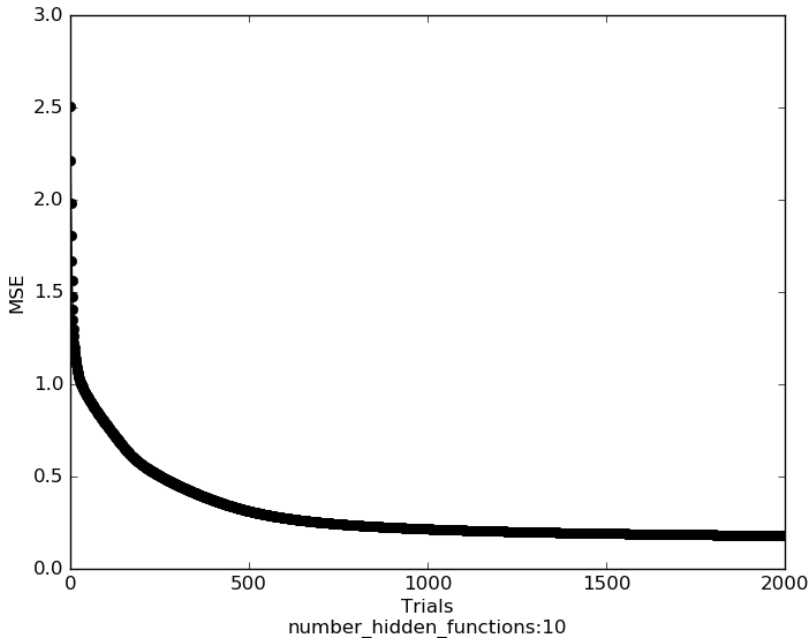

Figure 4.3: This graph depicts the learning curve of the RBF network when trained with the directional data at 0 db noise level.

the learning curve and the resulting performance on the validation set. The learning rate of the weight vector is chosen to be greater than the learning rate of the center vectors t and inverse matrix Σ^{-1}. With this setting, the weights of the output layer update rapidly while parameters of the hidden layer functions update slowly. The design parameters θ, t and Σ^{-1} are initialised with randomly chosen input vectors. The number of radial basis functions required for the directional antennas is less than that of the isotropic antennas. This implies that the decision boundary is less complex in the data obtained from directional antennas compared to that of isotropic antennas.

The learning curve of the RBF network during training with the directional data with 0 db noise level is shown in Fig. 4.3. The learning curve has converged after approximately 2000 iterations. The values of θ, t and Σ^{-1} at 2000 iteration are chosen as the parameters for the RBF network. With the other databases, similar trends are exhibited in the learning curve.

The performance of the classifiers is measured with the prediction rates (PR) from the testing data i.e., percentage of correct classifications with respect to the testing set size. The classification performance of the logistic regression and RBF networks with the data from different antenna designs and noise levels is shown in Table 4.2. The logistic regression was implemented in python using the `LogisticRegression` class from the `sklearn` linear model and with polynomial features of degree 2. In the scenario considered, the monitoring system with directional antennas provided better classification performance than the system with isotropic antennas. These results indicate that the information ob-

tained from the appropriately designed directional antennas is more discriminating than the isotropic antennas. Using antennas that are designed based on the target area and size will yield better performance results.

Table 4.2: Performance scores with simulation data.

Classifier	**Noise Level**	**Isotropic PR**	**Directional PR**
Logistic Regression	0db	92.52	98.80
Logistic Regression	2db	84.79	95.26
Logistic Regression	4db	78.95	90.67
RBF network	0db	92.20	97.42
RBF network	2db	85.40	95.03
RBF network	4db	80.02	91.30

5 EXPERIMENTAL CAMPAIGN

In numerical simulations, performance results are obtained using the data derived from the free space path loss model. To complement these findings, an experimental campaign is conducted in a line-of-sight environment to acquire field data. The field data is acquired under different radiation characteristics of the sensing devices. The experiment was implemented inside a 50 m $\times$ 50 m open space area in the parking lot 100j at Texas A&M university. In this experimental setting, the target area $\mathscr{A}_{\mathrm{t}}$ is considered to be a square of dimension 20 m $\times$ 20 m inscribed in a larger square of dimension 50 m $\times$ 50 m. This is the same scenario as the simulation framework. This chapter describes the experimental setup and discusses the performance results obtained from field measurements.

5.1 Distributed Wi-Fi Monitoring System

For this experiment, a distributed Wi-Fi monitoring system is designed to monitor wireless networks operating on the 2.4 GHz ISM radio band. The distributed monitoring system consists of four monitoring devices placed at the corners of the target area and a central server to integrate the information from all monitoring devices.

5.1.1 Monitoring Devices

Every monitoring device takes the form of a dedicated Next Unit of Computing (NUC) by Intel™ and it runs an instance of GNU/Linux as its operating system. Each NUC is equipped with two external wireless network interface cards with detachable an-

tennas. Wireless monitoring is enabled by setting these external network cards to monitoring mode. The functionality of an NUC is to decode the packets captured by the network interface cards and also to filter and store the packet information in a database. For this, a custom software is developed in C language using the `pcap` application programming interface (API). This software deciphers the transmitter MAC address and the RSSI information from the captured packets. For every pertinent packet, it stores the retrieved information along with the time stamp of the packet capture to a local SQLite database. This software filters redundant data using a hash table, which naturally removes duplicates within detected MAC addresses. The monitoring device set up is shown in Fig. 5.1.

Figure 5.1: Monitoring device setup with Intel™ NUC and custom antenna designs.

5.1.2 Monitoring Antennas

In this experimental setup, Alfa™ AWUS036NHA wireless interfaces are used as the external network cards. It enables operators to launch IEEE 802.11b/g/n wireless network at 150 Mbps in the 2.4GHz band, which is also compatible with IEEE 802.11b/g wireless devices at 54 Mbps. These interfaces are composed of a detachable antenna and an Atheros™ chipset. The Atheros™ chipset provides two modes of operation - Managed and Monitor. In monitoring mode, the chipset is capable of listening to all traffic present on a channel in a 2.4 GHz band.

The default antennas of the network cards attached to the NUC are replaced with custom designed isotropic and directional patch antennas. The custom designed antennas are depicted in Fig. 5.1. To reduce noise levels, the antennas are placed at a height of 5 ft from the ground using dowels and mounts for the NUCs. The mounts for the NUCs are designed using SolidWorks, and they are 3D printed with a Makerbot-2 device. The antennas are placed at different heights to reduce coupling among them. The NUCs are powered with extension cables using an inverter from a car.

5.1.3 Central Server

The central server is designed to collect and integrate information from all monitoring devices. In the experimental setup, the transfer of information from monitoring devices to the central server is made via the TCP protocol. At the central server, each wireless device is identified by its unique MAC address, and RSSI values belonging to a particular device are grouped together based on its MAC address. The fusion center possesses side

information in the form of the locations of sensing devices, their orientations and antenna properties. We use this data to study the effect of using directional and omni-directional antennae in the network cards and to compare their classification performance on the observed devices.

5.2 Wireless Agents

The wireless agents are Android™ smartphones and laptops with isotropic antennas. In this study, we assume that the wireless users are quasistatic and an inference task is performed over a single monitoring period. Although it is possible to incorporate moving agents and streaming observations into the problem formulation, these features render the analysis more challenging and they are not necessary to achieve our goal of better understanding the interplay between antenna profiles and RF monitoring. As such, advanced mobility models and their ramifications are relegated to future work in favor of a simpler, explicative model suited to our main purpose.

Throughout the course of the experiment, every wireless unit runs a custom app, which logs GPS coordinates and time. The app is required to establish a ground truth about each location. All the agents are operating on the same wireless network, and they periodically transmit the information collected by the app to a central location. MAC addresses and time stamps are then used to match locations to power vectors at the inference center, thereby establishing the desired ground truth.

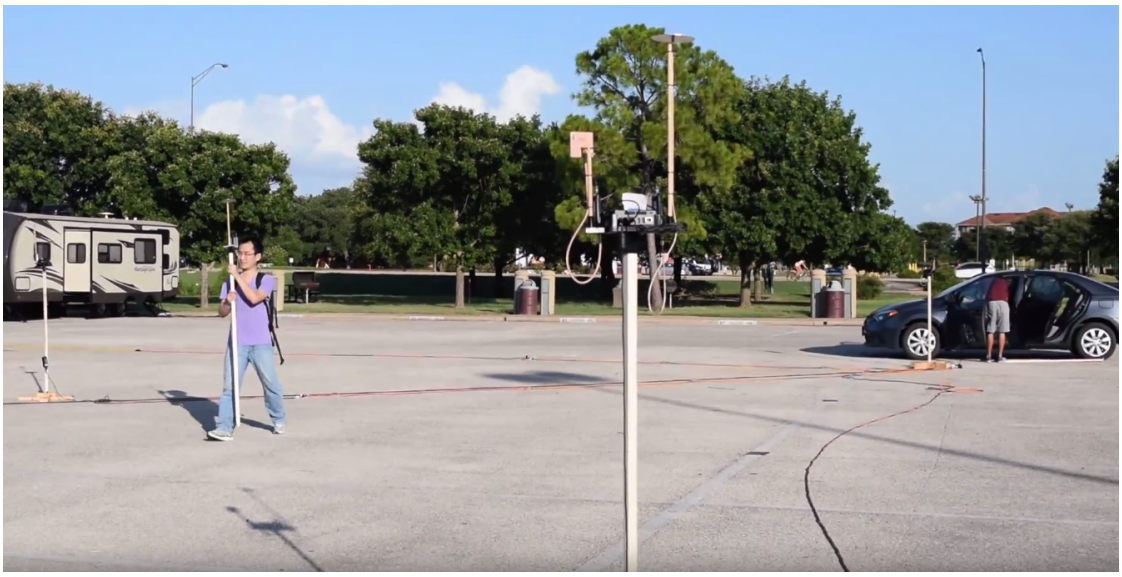

Figure 5.2: Experimental area.

5.3 Experimental Samples

Altogether, the experimental set contains approximately 800 power and location vectors for monitoring devices with isotropic antennas, and another 800 power and location vectors for a system with directional antennas. Since there are four monitoring devices, this is equivalent to 6,400 distinct points. For every location inside the overall region, the signal strengths received at the four monitoring units are aggregated into a single vector p, which serves as input to the classification algorithms. The estimates are then compared with the ground truth derived from the known locations. The locations of the data points obtained from the field experiment are shown in Fig. 5.2. The red marks indicate the locations of monitoring units and the green dots indicate the locations of the collected data points.

Figure 5.3: Sample locations for the acquired data during the field experiment.

5.4 Experimental Results

The performance results obtained from the experimental data are shown in Table 5.1. The experimental results show similar findings as that of the numerical simulations. While comparing numerical simulations with experimental data, one should keep in mind a few considerations. The locations afforded by the GPS units of the smartphones only form an approximate ground truth because the readings suffer from inaccuracies on the order of 2 m. In numerical simulations, synthetic data is generated assuming that the wireless agents possess isotropic antennas whereas commercial smart phones have arbitrary radiation patterns. These issues point to the distinctions between synthetic and experimental data. Nevertheless, in the framework considered herein, the classification performance of

the monitoring systems with directional antennas is far better than that of the systems with omnidirectional antennas. This analysis clearly shows the advantages of using directional antennas over isotropic antennas in the scenario considered. In general, custom antennas can be designed based on the inference task, shape and size of the monitoring region, leading to significant performance gains.

Table 5.1: Performance scores with field data.

Classifier	**Isotropic P.R**	**Directional P.R**
Logistic Regression	75.15	88.30
RBF network	76.02	89.12

6 CONCLUSION

Wireless devices with Wi-Fi enabled cards periodically transmit probe signals to obtain information about nearby access points. Such messages incorporate information about the identity of the immediate transmitter and they can be monitored passively using certain network interface cards in monitoring mode. In this work, a distributed Wi-Fi monitoring system is designed to accurately estimate the number of active agents present within a region of interest based on Wi-Fi activity. An important consideration in assessing the performance of inference tasks based on such monitoring systems is the design of the antennas attached to the sensing devices. The performance of a distributed monitoring system can be enhanced by using antenna designs that collectively strongly discriminate between the possible locations of the wireless agents. This work evaluates the performance of the occupancy estimation with the data obtained from monitoring systems with isotropic and directional antennas. The findings clearly show the advantages of using directional antennas over isotropic antennas in the scenario considered. This work suggests that utilizing custom designed antennas based on the inference, shape, and size of the target region can significantly improve the performance of a Wi-Fi monitoring system.

REFERENCES

[1] Cisco Systems, Inc., *Visual Networking Index: Global Mobile Data Traffic Forecast Update*, 2016.

[2] N. Patwari and J. Wilson, "RF sensor networks for device-free localization: Measurements, models, and algorithms," *Proc. IEEE*, vol. 98, no. 11, pp. 1961–1973, 2010.

[3] J. Shen, A. F. Molisch, and J. Salmi, "Accurate passive location estimation using TOA measurements," *IEEE Trans. Wireless Commun.*, vol. 11, no. 6, pp. 2182–2192, 2012.

[4] A. B. M. Musa and J. Eriksson, "Tracking unmodified smartphones using Wi-Fi monitors," in *Conference on Embedded Network Sensor Systems*, pp. 281–294, ACM, 2012.

[5] Y. Wang, J. Yang, H. Liu, Y. Chen, M. Gruteser, and R. P. Martin, "Measuring human queues using WiFi signals," in *International Conference on Mobile Computing & Networking*, pp. 235–238, ACM, 2013.

[6] M. V. Barbera, A. Epasto, A. Mei, V. C. Perta, and J. Stefa, "Signals from the crowd: Uncovering social relationships through smartphone probes," in *Internet Measurement Conference*, pp. 265–276, ACM, 2013.

[7] A. H. Sayed, A. Tarighat, and N. Khajehnouri, "Network-based wireless location: challenges faced in developing techniques for accurate wireless location information," *IEEE Signal Process. Mag.*, vol. 22, no. 4, pp. 24–40, 2005.

[8] N. Patwari, J. N. Ash, S. Kyperountas, A. O. Hero III, R. L. Moses, and N. S. Correal, "Locating the nodes: cooperative localization in wireless sensor networks," *IEEE Signal Process. Mag.*, vol. 22, no. 4, pp. 54–69, 2005.

[9] P. M. Djurić, M. Vemula, and M. F. Bugallo, "Target tracking by particle filtering in binary sensor networks," *IEEE Trans. Signal Process.*, vol. 56, no. 6, pp. 2229–2238, 2008.

[10] H. Wymeersch, J. Lien, and M. Z. Win, "Cooperative localization in wireless networks," *Proceedings of the IEEE*, vol. 97, no. 2, pp. 427–450, 2009.

[11] O. Ozdemir, R. Niu, and P. K. Varshney, "Channel aware target localization with quantized data in wireless sensor networks," *IEEE Trans. Signal Process.*, vol. 57, no. 3, pp. 1190–1202, 2009.

[12] J. Wang, R. K. Ghosh, and S. K. Das, "A survey on sensor localization," *Journal of Control Theory and Applications*, vol. 8, no. 1, pp. 2–11, 2010.

[13] A. Vempaty, O. Ozdemir, K. Agrawal, H. Chen, and P. K. Varshney, "Localization in wireless sensor networks: Byzantines and mitigation techniques," *IEEE Trans. Signal Process.*, vol. 61, no. 6, pp. 1495–1508, 2013.

[14] J. M. Smith and D. Towsley, "The use of queuing networks in the evaluation of egress from buildings," *Environment and Planning B: Planning and Design*, vol. 8, no. 2, pp. 125–139, 1981.

[15] Y. Agarwal, B. Balaji, R. Gupta, J. Lyles, M. Wei, and T. Weng, "Occupancy-driven energy management for smart building automation," in *Workshop on Embedded Sensing Systems for Energy-Efficiency in Building*, pp. 1–6, ACM, 2010.

[16] S.-F. Lin, J.-Y. Chen, and H.-X. Chao, "Estimation of number of people in crowded scenes using perspective transformation," *IEEE Transactions on Systems, Man, and Cybernetics-Part A: Systems and Humans*, vol. 31, no. 6, pp. 645–654, 2001.

[17] M. Kim, W. Kim, and C. Kim, "Estimating the number of people in crowded scenes," in *IS&T/SPIE Electronic Imaging*, pp. 78820L–78820L, International Society for Optics and Photonics, 2011.

[18] S. Depatla, A. Muralidharan, and Y. Mostofi, "Occupancy estimation using only wifi power measurements," *IEEE Journal on Selected Areas in Communications*, vol. 33, no. 7, pp. 1381–1393, 2015.

[19] F. M. Naini, O. Dousse, P. Thiran, and M. Vetterli, "Opportunistic sampling for joint population size and density estimation," *IEEE Trans. Mobile Comput.*, vol. 14, no. 12, pp. 2530–2543, 2015.

[20] D. Li, K. D. Wong, Y. H. Hu, and A. M. Sayeed, "Detection, classification, and tracking of targets," *IEEE Signal Process. Mag.*, vol. 19, no. 2, pp. 17–29, 2002.

[21] X. Sheng and Y. H. Hu, “Maximum likelihood multiple-source localization using acoustic energy measurements with wireless sensor networks,” *IEEE Trans. Signal Process.*, vol. 53, no. 1, pp. 44–53, 2005.

[22] Technical Specification Group Radio Access Network, 3rd Generation Partnership Project, *Spatial Channel Model for Multiple Input Multiple Output (MIMO) Simulations*, 2011. release 10.